Supporting Information

Atomically dispersed Fe atoms anchored on COF-derived N-doped carbon nanospheres as efficient multi-functional catalysts

Shengjie Wei[+], Yu Wang[+], Wenxing Chen, Zhi Li*, Weng-Chon Cheong, Qinghua Zhang, Yue Gong, Lin Gu, Chen Chen, Dingsheng Wang, Qing Peng and Yadong Li*

Experimental Section

Reagents*:* 1,3,5-tris(4-aminophenyl) benzene (Shanghai Dibai, http://www.chemxyz.com), 1,3,5-benzenetricarboxaldehyde (Shanghai Bide, www.bidepharm.com), methanol (Beijing Chemical Reagent), ethanol (Beijing Chemical Reagent), acetone (Beijing Chemical Reagent), acetonitrile (Beijing Chemical Reagent), acetic acid (Beijing Chemical Reagent), $FeCl_3 \cdot 6H_2O$ (http://tjsjkjxhgyjs.china.herostart.com), Cobalt acetoacetate (Alfa Aesar), Nickel acetoacetate (Alfa Aesar), Iron(III) acetylacetonate (Alfa Aesar), borane-tert-butylamine (TCI), oleylamine (aldrich), cyclohexane (tgchem), Ethylbenzene (Alfa Aesar), n-Dodecane (TCI), tert-butyl hydroperoxide (70% aqueous solution) (Macklin), 1,2,3,4-tetrahydroquinoline (aladdin) and mesitylene (aladdin), Nafion D-521 dispersion (5% w/w in water and 1-propanol) (Alfa Aesar), commercial Pt/C (20 wt% metal, Alfa Aesar), KOH (analytical grade, Sinopharm Chemical). The distilled water used in ORR reaction was obtained through ion-exchange and filtration.

Preparation of RT-COF-1[1]: We mixed 30 mL methanol and 30mL acetone with vigorous stirring at room temperature. Then, 205 mg 1,3,5-tris(4-aminophenyl) benzene and 95 mg 1,3,5-benzenetricarboxaldehyde were poured in the above solution and dissolved under ultrasonic for several minutes. We added 6mL glacial acetic acid (≥99.5%) in the solution under vigorous stirring for 15 minutes. We collected the obtained RT-COF-1 powder by centrifugation at 16,000 rpm for 5 min. We washed and collected the RT-COF-1 powder with methanol by centrifugation at 16,000 rpm for 5 min for three times.

Preparation of Fe-ISAS/CN: We dissolved 30 mg RT-COF-1 powder in 10mL acetonitrile. Then, we dropped 0.029mL $FeCl_3 \cdot 6H_2O$ acetonitrile solution (10mg $FeCl_3 \cdot 6H_2O$ /mL) in the above solution with vigorous stirred under room temperature for 24 hours. After fully absorption, we collected the iron ions-doped RT-COF-1 powder by centrifugation at 16,000 rpm for 5 min without washing any more. We dried the product for several hours at 80°C. Then we transferred the iron ions-doped RT-COF-1 powder into a ceramic boat and placed it in a tube furnace. The sample was heated to 900°C with a heating rate of 5°C/min and we kept the temperature for three hours under flowing nitrogen gas and then we cooled the sample naturally to room temperature. The preparation of Fe/CN is similar to that of Fe-ISAS/CN and the only difference is that 0.730mL $FeCl_3 \cdot 6H_2O$ acetonitrile solution (10mg $FeCl_3 \cdot 6H_2O$ /mL) was added.

Preparation of Co-ISAS/CN: We dissolved 30 mg RT-COF-1 powder in 10mL acetonitrile. Then, we dropped 0.267mL cobalt acetoacetate acetonitrile solution (1mg cobalt acetoacetate /mL) in the above solution with vigorous stirred under room temperature for 24 hours. After fully absorption, we collected the cobalt ions-doped RT-COF-1 powder by centrifugation at 16,000 rpm for 5 min without washing any more. We dried the product for several hours at 80°C. Then we transferred the cobalt ions-doped RT-COF-1 powder into a ceramic boat and placed it in a tube furnace. The sample was heated to 900°C with a heating rate of 5°C/min and we kept the temperature for three hours under flowing nitrogen gas and then we cooled the sample naturally to room temperature.

Preparation of Ni-ISAS/CN: We dissolved 30 mg RT-COF-1 powder in 10mL acetonitrile. Then, we dropped 0.267mL nickel acetoacetate acetonitrile solution (1mg nickel acetoacetate /mL) in the above solution with vigorous stirred under room temperature for 24 hours. After fully absorption, we collected the nickel ions-doped RT-COF-1 powder by centrifugation at 16,000 rpm for 5 min without washing any more. We dried the product for several hours at 80^{o}C. Then we transferred the nickel ions-doped RT-COF-1 powder into a ceramic boat and placed it in a tube furnace. The sample was heated to 900^{o}C with a heating rate of 5^{o}C/min and we kept the temperature for three hours under flowing nitrogen gas and then we cooled the sample naturally to room temperature.

Preparation of COF-derived CN: We transferred the pure RT-COF-1 powder into a ceramic boat and placed it in a tube furnace. The sample was heated to 900^{o}C with a heating rate of 5^{o}C/min and kept the temperature for three hours under flowing nitrogen gas and we cooled the sample naturally to room temperature.

Preparation of Fe-NPs/CN: The Fe nanoparticles were prepared by a reported article.[2] We dissolved 20mg Iron(III) acetylacetonate in 10 mL oleylamine at 250 ^{o}C under vigorous stirring for 10 minutes. Then, we added a solution of 100 mg borane-tert-butylamine dissolved in 2 mL oleylamine quickly into the above solution. After two minutes, we heated the flask to 270 ^{o}C and keep the temperature for an hour. After the solution was cooled to room temperature naturally, we washed the solution with ethanol and then dispersed the Fe nanoparticles in 3.163 mL cyclohexane for

future use. We dissolved 100 mg COF-derived CN powder in 5 mL ethanol under ultrasonic. Then we dropped 0.5 mL above Fe nanoparticles/cyclohexane solution under vigorous stir for 12 hours. We collected the Fe-NPs/CN sample by centrifugation at 16,000 rpm for 5 min without washing. The obtained Fe-NPs/CN was dried at 30^{o}C under vacuum.

Characterization

We measured crystalline structure and phase purity by utilizing Rigaku RU-200b X-ray powder diffractometer (XRD) with CuKα radiation (λ= 1.5418Å). The metal concentrations of the samples was investigated by inductively coupled plasma optical emission spectrometry (ICP-OES). We carried out STEM observation by using a probe aberration-corrected microscope, JEM-ARM200F equipped with a cold emitter, operated at 200kV. The microscope has an attainable spatial resolution of 78pm. The atomic structure of the samples were characterized using an ARM-200CF (JEOL, Tokyo, Japan) transmission electron microscope operated at 200 keV and equipped with double spherical aberration (Cs) correctors. The attainable resolution of the probe defined by the objective pre-field is 78 picometers.

XAFS measurement: The X-ray absorption fine structure measurement was carried out at BL14W1 station in Shanghai Synchrotron Radiation Facility (SSRF, operated at 3.5 GeV with a maximum current of 250 mA, Fe, Co and Ni K-edge). We collected the XAFS data at room temperature in fluorescence mold by utilizing ionization chamber. All the powder of samples was pelletized as a disks with a

diameter of 8mm by using polyvinylidene fluoride (PVDF) powder which serve as binders. We collected all spectra in ambient conditions.

XAFS Analysis and Results: We analyzed the obtained EXAFS data according to the standard procedures by the analysis of the ATHENA module of the IFEFFIT software packages. We processed the obtained EXAFS spectra by subtracting post-edge background from the overall absorption and normalizing according to the edge-jump step. Then, theχ(k) data was transformed to real (R) space by utilization of a hanning windows (dk=1.0 Å-1) for the separation of the EXAFS contributions from different coordination shells. Least-squares curve parameter fitting was carried out by utilization of the ARTEMIS module of the IFEFFIT software packages in order to obtain the quantitative structural parameters around central metal atom.[3]

The EXAFS equation was listed below:

$$\chi(k)=\sum_j \frac{N_j S_o^2 F_j(k)}{k R_j^2}\exp[-2k^2\sigma_j^2]\exp[\frac{-2R_j}{\lambda(k)}]\sin[2kR_j+\phi_j(k)]$$

In the above equation, S_0^2 represented the amplitude reduction factor. $F_j(k)$ represented the effective curved-wave backscattering amplitude. N_j represented the number of neighbors in the j_{th} atomic shell. R_j represented the distance between the X-ray absorbing central atom and the atoms in the j_{th} atomic shell (backscatterer). λ represented the mean free path in Å. σ_j represented the Debye-Waller parameter of the jth atomic shell (variation of distances around the average R_j). $\phi_j(k)$ represented the phase shift (including the phase shift for each shell and the total central atom phase

shift). We calculated the functions $F_j(k)$, λ and $\phi_j(k)$ with the ab initio code FEFF8.2.[4] We listed the additional details for EXAFS simulations below.

The S_0^2 value was 0.85 and was fixed in the subsequent fitting of Fe, Co and Ni K-edge, while the internal atomic distances R, the edge-energy shift ΔE_0 and Debye-Waller factor σ^2 were allowed to work separately. The obtained parameters of Fe, Co and Ni K-edge were listed in Table S2.

Electro-catalytic Measurement

We prepared all catalysts by mixing 5 mg of the catalyst in 1 ml of solution which contain 490 μL of ethanol, 490 μL of H2O and 20 μL of 5% Nafion solution. Then, the solution was treated by ultrasonication for 1 h in order to form homogeneous catalyst inks. The commercial 20 wt% Pt/C was also prepared as a 5 mg/mL solution by the above treatment. For obtaining a desirable catalyst loading, we carefully dropped a certain volume of the catalyst ink on the polished glassy carbon rotating disk electrode (RDE) or rotating ring disk electrode (RRDE) to assure that the electrode was fully covered. The loading of nonprecious metal-based catalyst was 0.510 mg cm^{-2} and the loading of commercial 20wt% Pt/C was 0.127 mg cm^{-2}.

We carried out the electrochemical measurements by using a three-electrode system on a CHI 760E electrochemical workstation (Shanghai Chenhua, China) in 0.1 M KOH electrolyte. A rotating disk electrode (RDE) with a glassy carbon (GC) disk of 5 mm in diameter and a rotating ring-disk electrode with a Pt ring (6.5 mm inner diameter and 8.5 mm outer diameter) served as the working electrode. We utilized a

carbon rod as counter electrode. We recorded the potential by using a Ag/AgCl (saturated KCl solution) electrode as the reference electrode. Before electrochemical measurement, oxygen flow was passed through the electrolyte in the cell for at least 30 minutes to make sure the solution was saturated with O_2, and all electrochemical experiments were conducted at room temperature. Linear sweep voltammetry (LSV) measurements were recorded at various rotating speed from 400 to 2500 rpm with a scan rate of 10 $mV \cdot s^{-1}$, and the cyclic voltammetry (CV) experiments were performed with a scan rate of 50 $mV \cdot s^{-1}$.

For the ORR at a RDE, the electron transfer number (n) and kinetic current density (J_k) were calculated according to the Koutecky-Levich equation as below:

$$\frac{1}{J} = \frac{1}{J_L} + \frac{1}{J_K} = \frac{1}{B\omega^{\frac{1}{2}}} + \frac{1}{J_K} \quad (1)$$

$$B = 0.62nFC_0 D_0^{\frac{2}{3}} V^{-\frac{1}{6}} \quad (2)$$

In the above equation, J represented the measured current density, J_K and J_L were the kinetic and limiting current densities, respectively. ω represented the angular velocity of the disk. n was the electron transfer number and F was the Faraday constant and its value was 96485 $C \cdot mol^{-1}$. C_0, D_0 and V represented the bulk concentration of O_2 (1.2×10^{-6} $mol \cdot cm^{-3}$), the diffusion coefficient of O_2 (1.9×10^{-5} $cm^2 \cdot s^{-1}$), and the kinematic viscosity of the electrolyte (0.01 $cm^2 \cdot s^{-1}$), respectively.

In the hydrogen peroxide yield tests, the disk electrode of RRDE was scanned catholically at a rate of 10 $mV \cdot s^{-1}$ and we set the ring electrode potential to 1.23 V vs.

RHE. We calculated the hydrogen peroxide yield (H_2O_2%) and the electron transfer number (n) by utilization of the following equations:

$$H_2O_2\,(\%) = 200 \times \frac{\frac{I_r}{N}}{I_d + \frac{I_r}{N}} \quad (3)$$

$$n = 4 \times \frac{I_d}{I_d + \frac{I_r}{N}} \quad (4)$$

In the above equation, I_d and I_r were the disk current and ring current, respectively. N was the current collection efficiency of the Pt ring and its value was 0.4.

We carried out the durability tests of the catalysts in the O_2-saturated 0.1 M KOH electrolyte at room temperature by performing potential cycling between 0.6 and 1.0 V vs. RHE. at a sweep rate of 50 $mV \cdot s^{-1}$ for 5,000 cycles.

Organic catalytic evaluation

In the selective oxidation of ethylbenzene toward acetophenone, we introduced ethylbenzene (0.5 mmol), catalyst (20.0 mg), TBHP (1.0 mL, 70 wt% in water), and water (2 mL) into a 15 mL Shlenck tube which was sealed with a Teflon lid at 60^{o}C for 24 hours under moderate stir. After catalysis, we extracted the organic substance with ethyl acetate and separated the solution and the solid catalysts by centrifugation. Then, the solid catalyst was washed by ethyl acetate and was collected by

centrifugation for the usage of next cycle. We analyzed the products with GC-MS and GC with n-Dodecane serving as an internal standard.

In the dehydrogenation of 1,2,3,4-tetrahydroquinoline, we introduce 1,2,3,4-tetrahydroquinoline (0.1mmol), catalyst (80.0 mg) and 1.5mL mesitylene into a 15 mL Shlenck tube which was sealed with a Teflon lid at 120^{o}C for 24 hours under moderate stir. After catalysis, we extracted the organic substance with ethyl acetate and separated the solution and the solid catalysts by centrifugation. Then, the solid catalyst was washed by ethyl acetate and was collected by centrifugation for the usage of next cycle. We analyzed the products with GC-MS and GC with n-Dodecane serving as an internal standard.

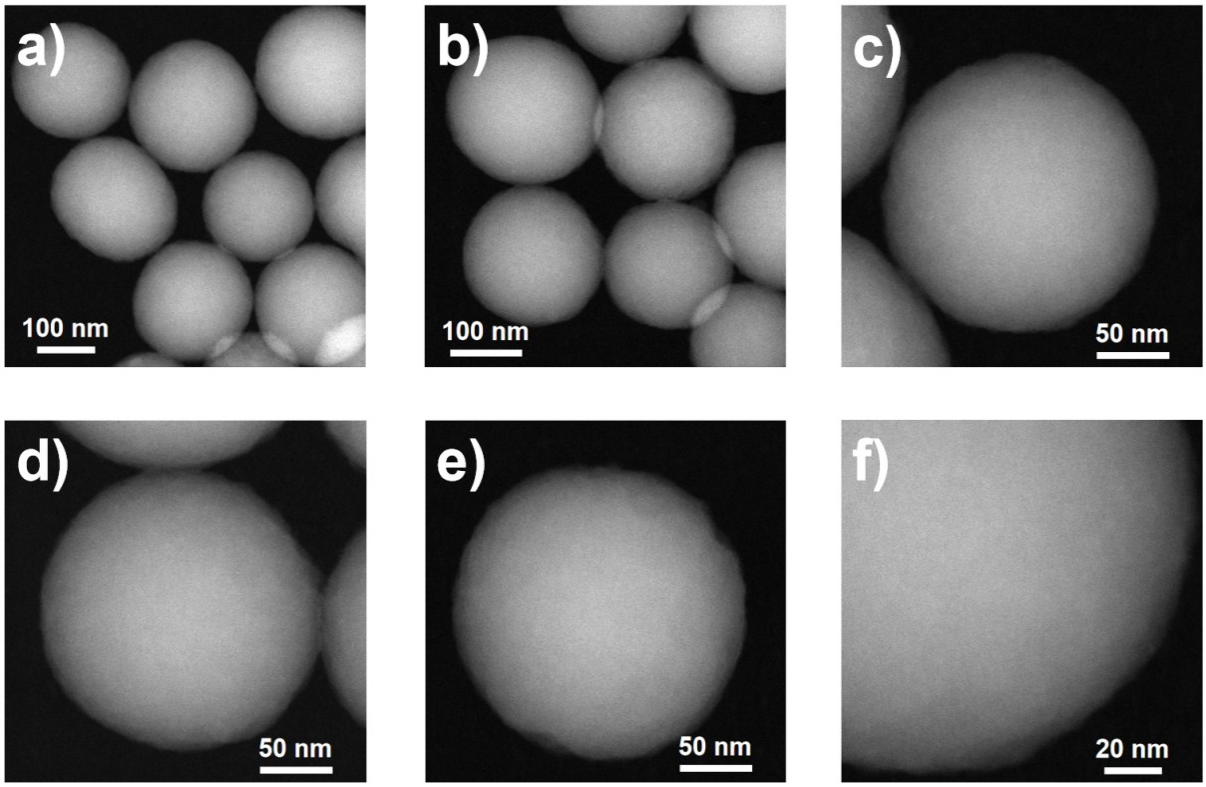

Figure S1. a) - f), The HAADF-STEM images of Fe-ISAS/CN from different regions at different magnifications.

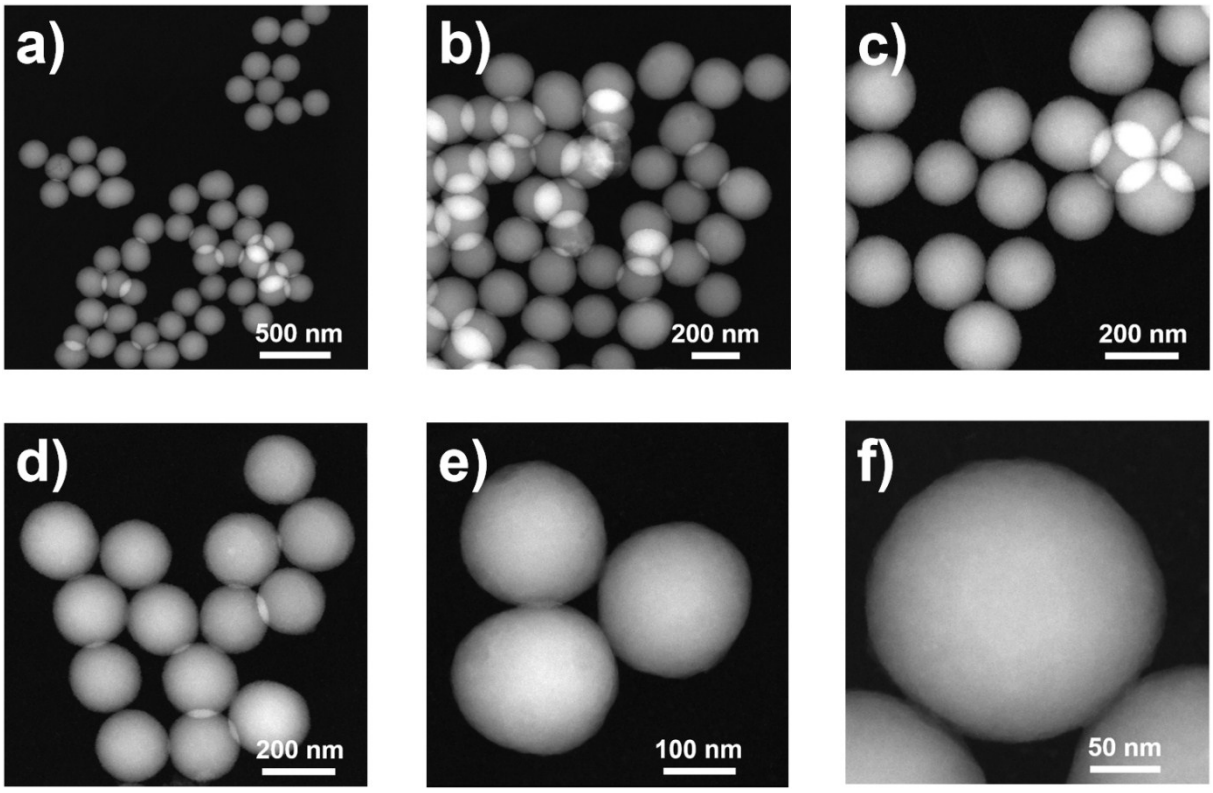

Figure S2. a) - f), The HAADF-STEM images of Co-ISAS/CN from different regions at different magnifications.

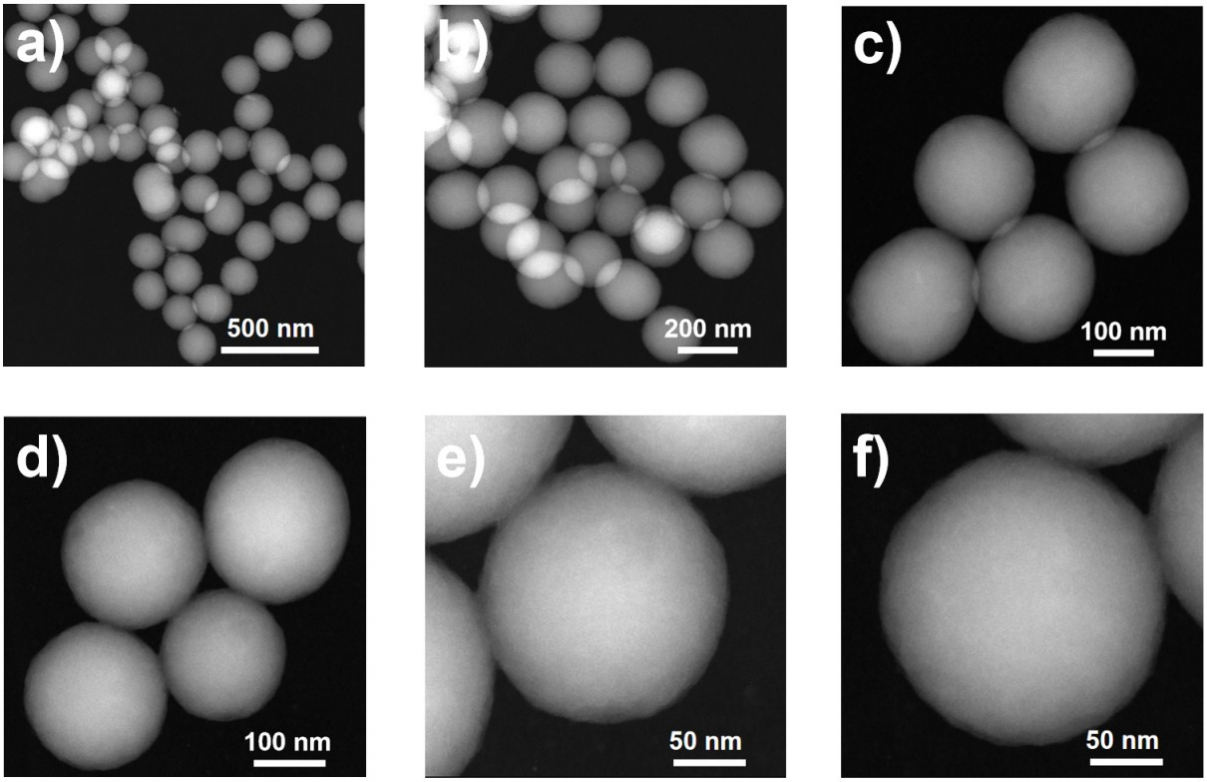

Figure S3. a) - f), The HAADF-STEM images of Ni-ISAS/CN from different regions at different magnifications.

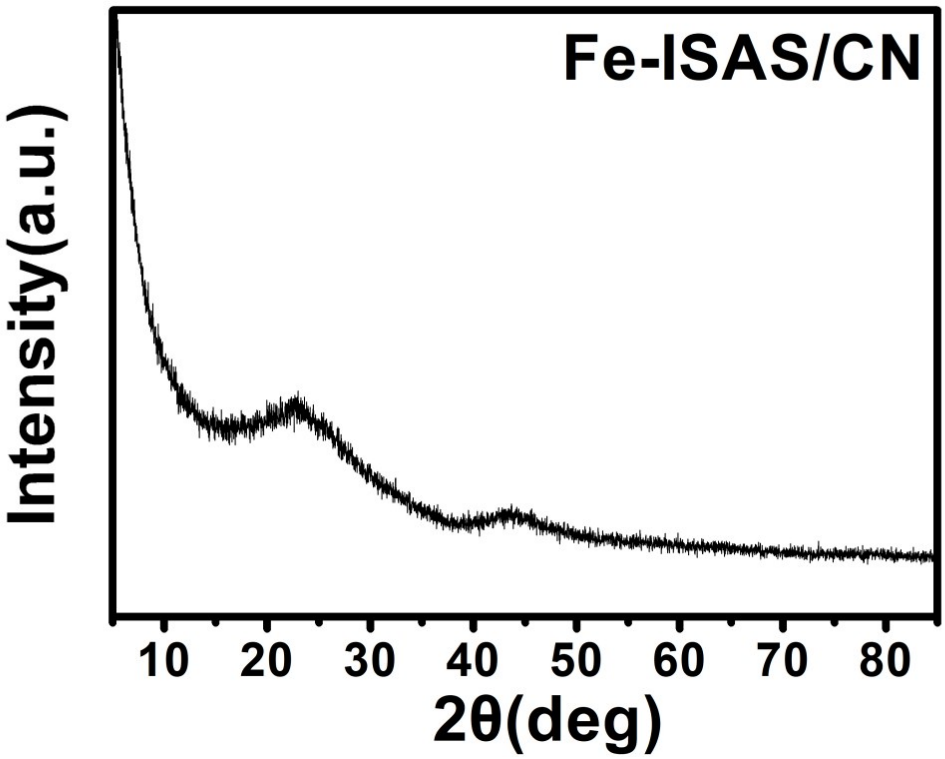

Figure S4. The XRD pattern of Fe-ISAS/CN.

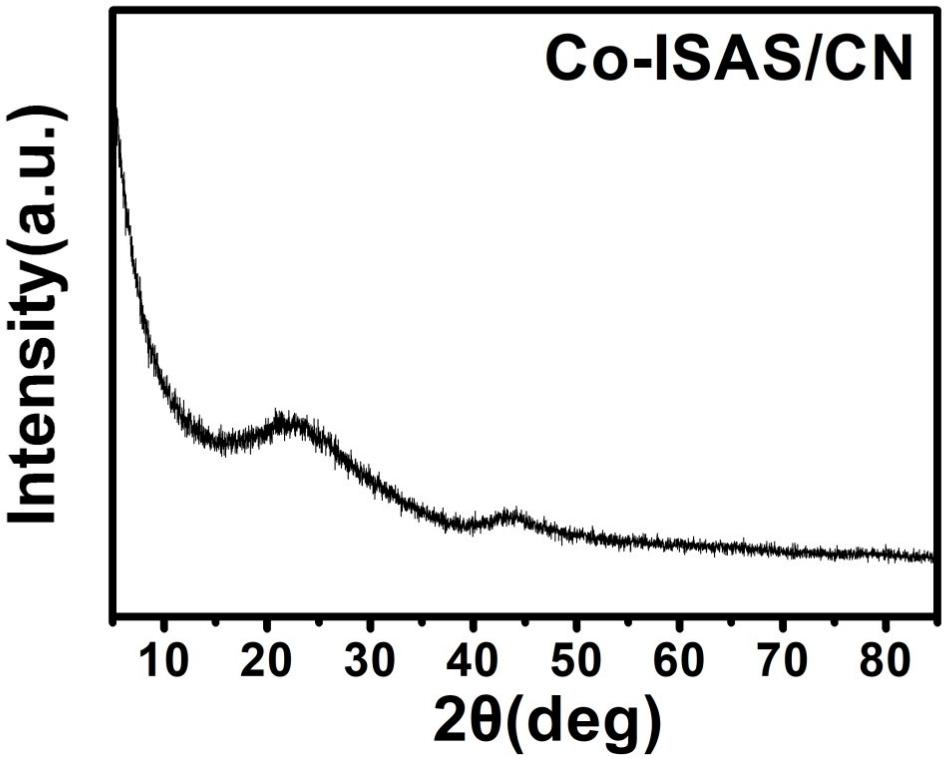

Figure S5. The XRD pattern of Co-ISAS/CN.

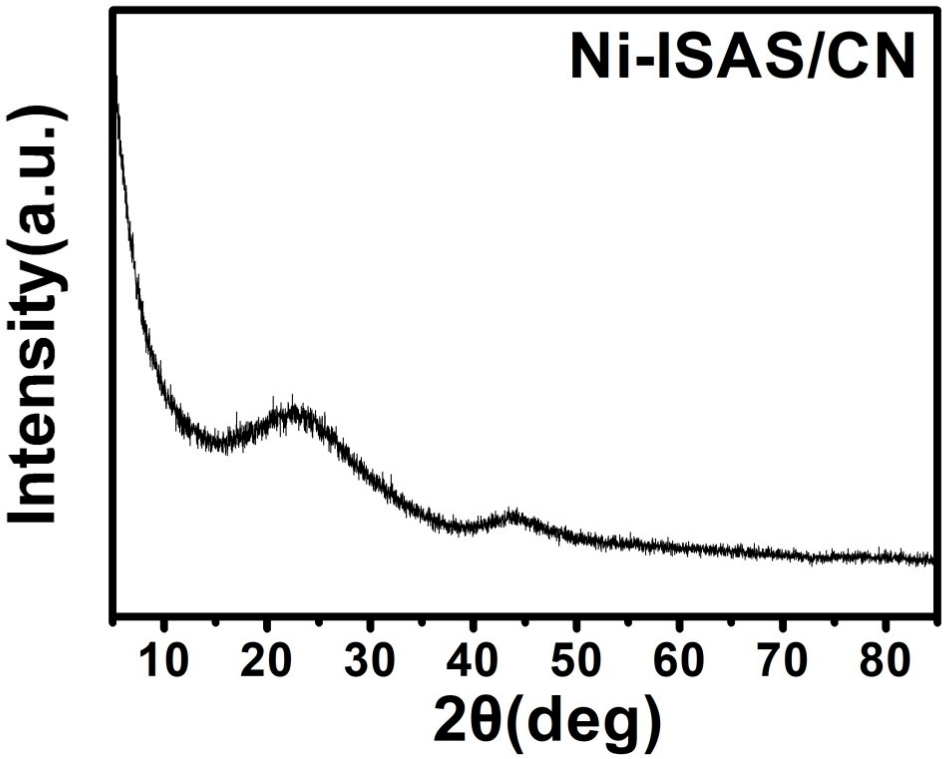

Figure S6. The XRD pattern of Ni-ISAS/CN.

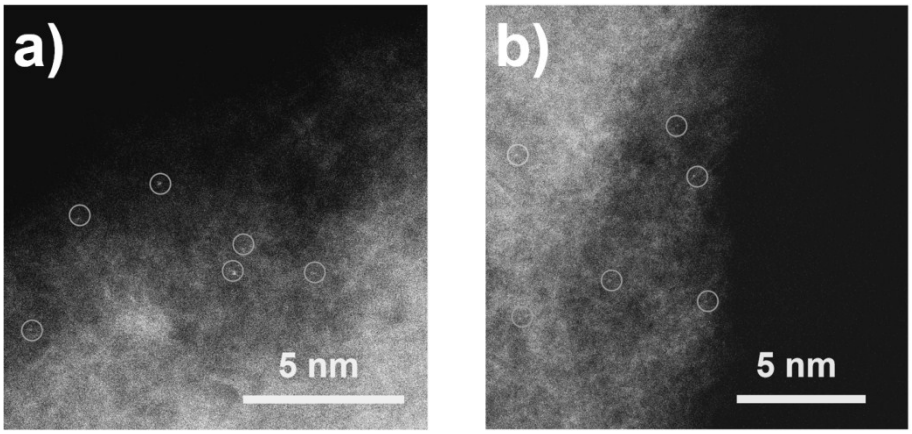

Figure S7. a) - b) High-resolution HAADF-STEM images of Fe-ISAS/CN in randomly selected regions.

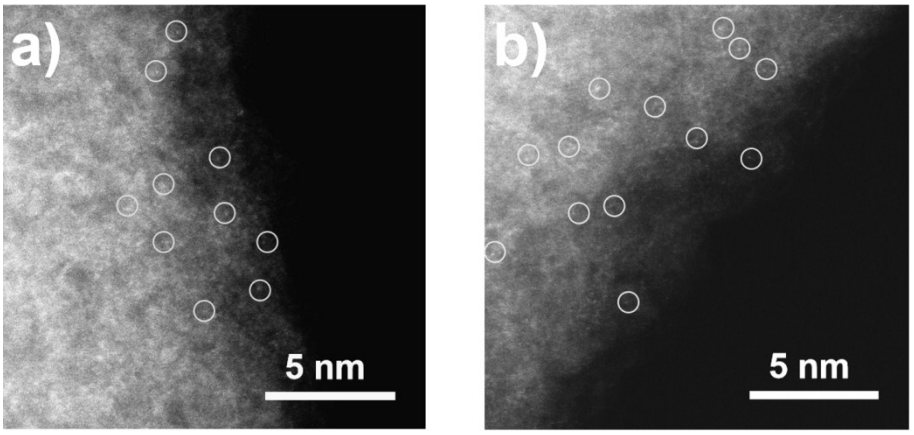

Figure S8. a) - b) High-resolution HAADF-STEM images of Co-ISAS/CN in randomly selected regions.

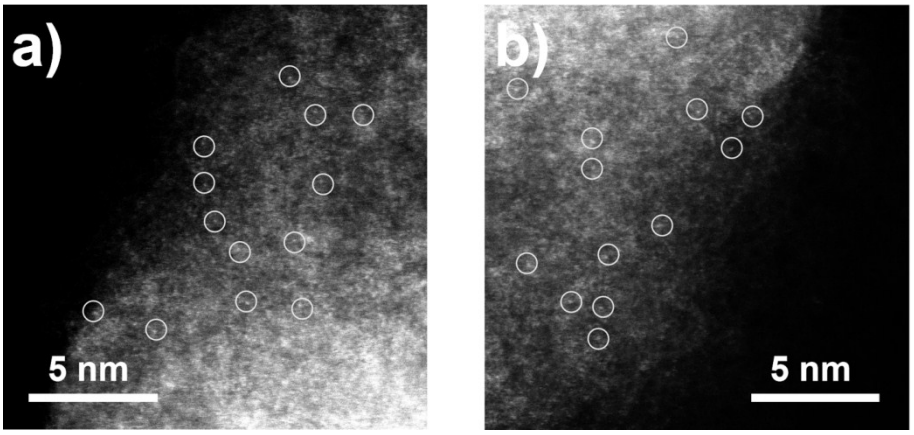

Figure S9. a) - b) High-resolution HAADF-STEM images of Ni-ISAS/CN in randomly selected regions.

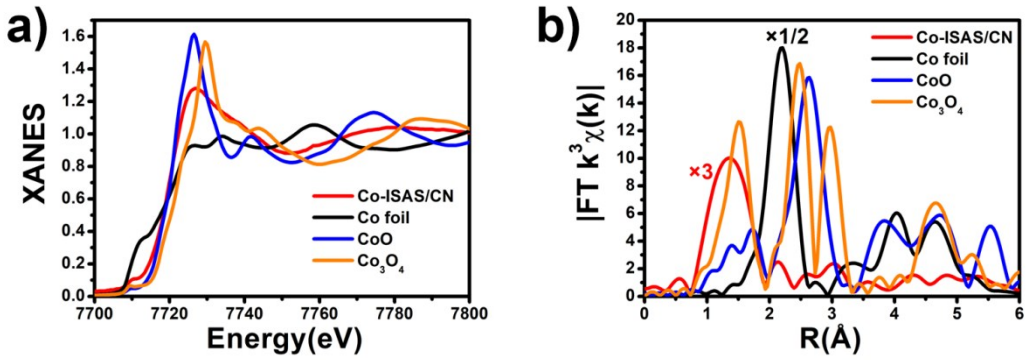

Figure S10. a)-b), The XANES spectrum of Co-ISAS/CN, Co foil, CoO and Co_3O_4 as reference samples and corresponding FT-EXAFS spectrum in R space.

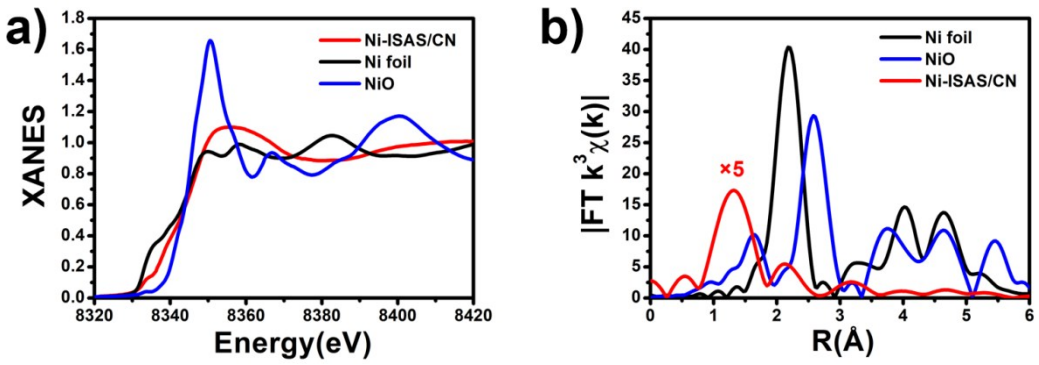

Figure S11. a) - b), The XANES spectrum of Ni-ISAS/CN, Ni foil and NiO as reference samples and corresponding FT-EXAFS spectrum in R space.

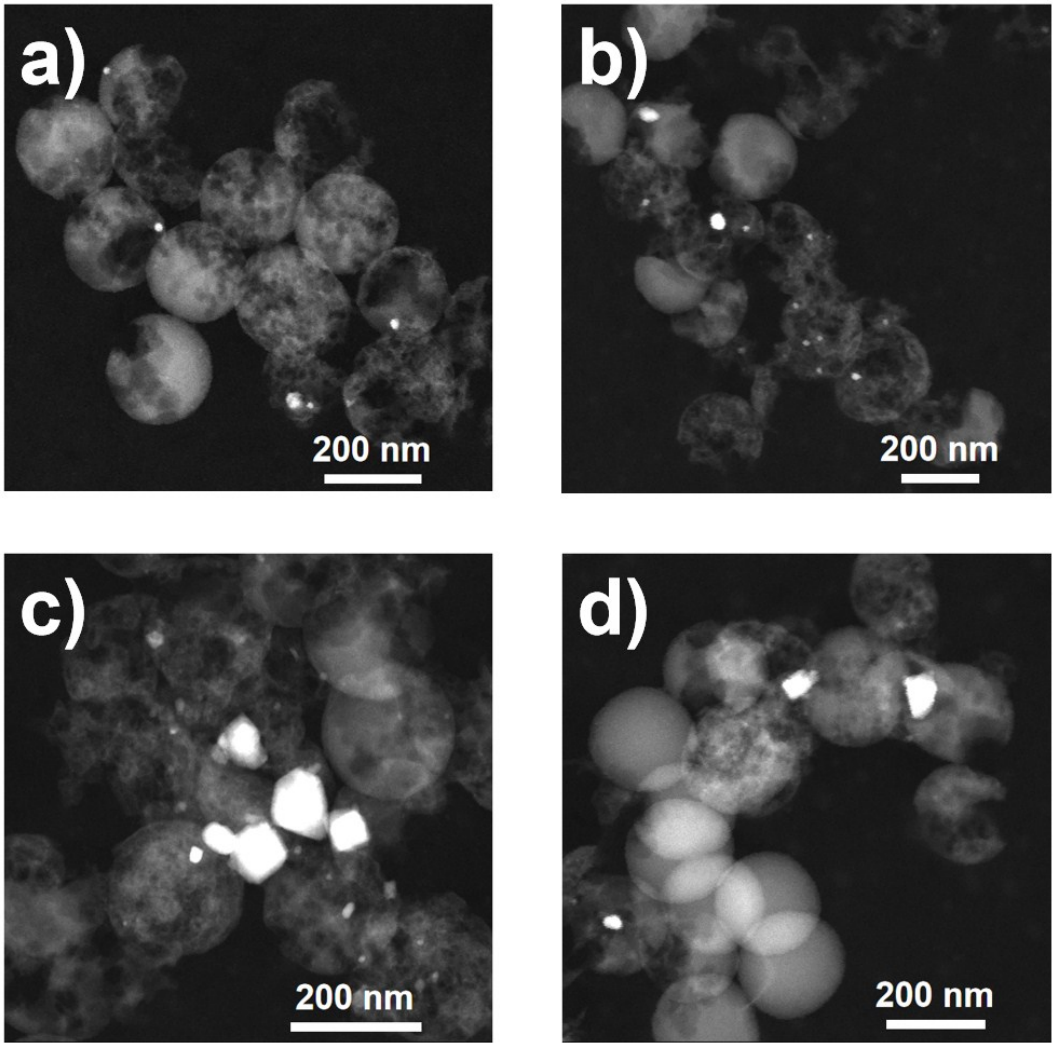

Figure S12. a) - d), The HAADF-STEM images of Fe/CN from different regions.

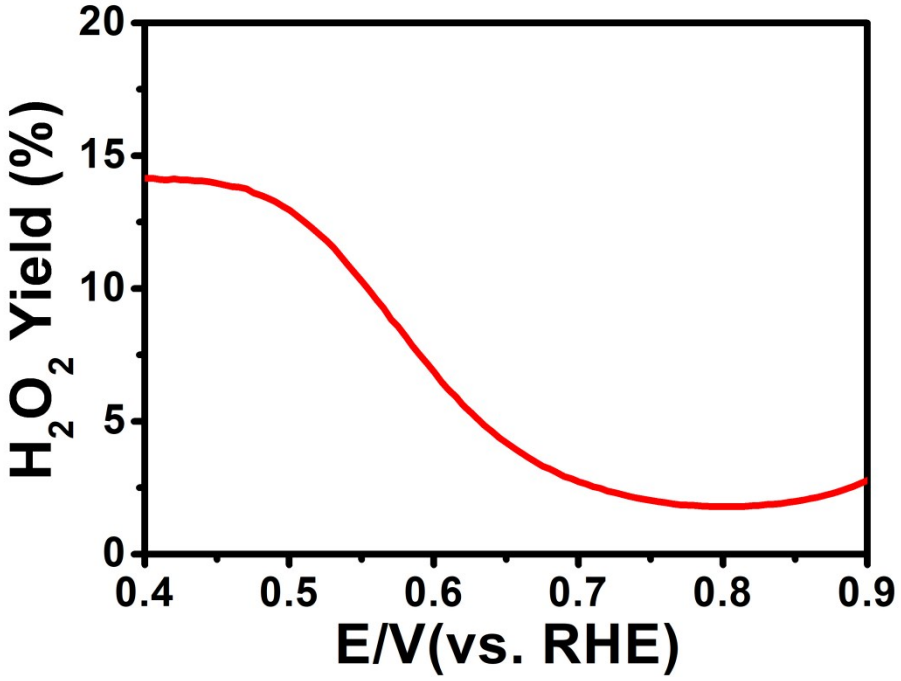

Figure S13. The H_2O_2 yiled of Fe-ISAS/CN was measured by using rotating ring disk electrode.

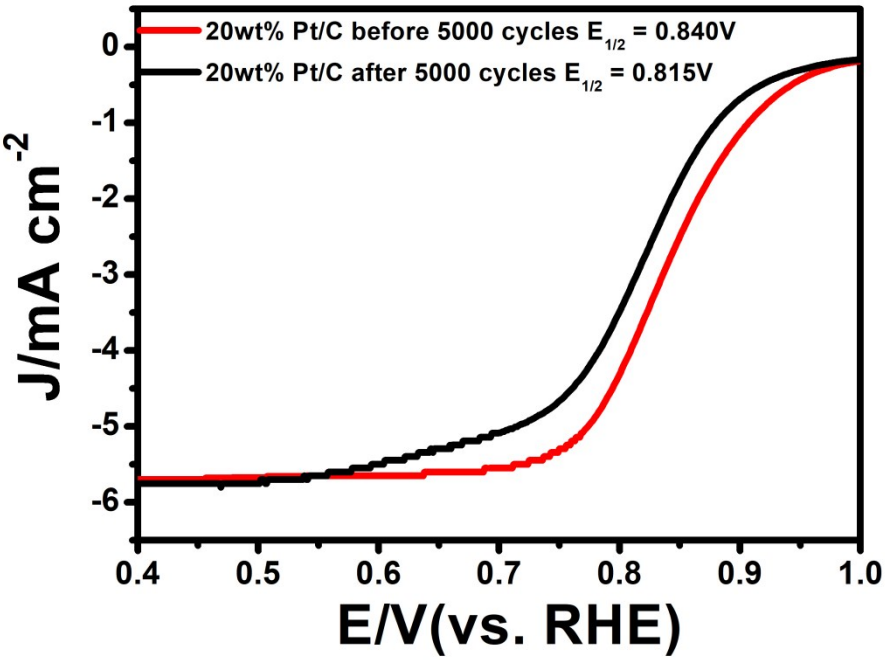

Figure S14. The comparison between the catalytic performance of commercial 20wt% Pt/C during the stability test in ORR reaction before and after 5000 cycles.

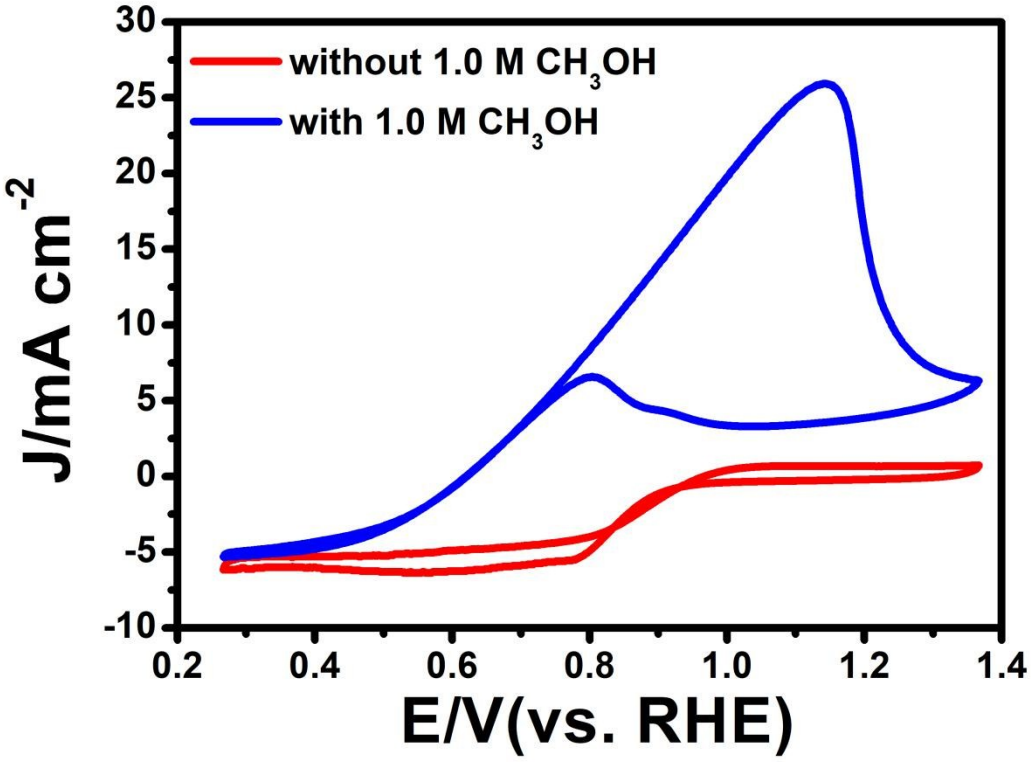

Figure S15. The comparison of CV curves of commercial 20wt% Pt/C in O_2-saturated 0.1M KOH without and with 1.0M CH_3OH at a scan rate of 50mV/s.

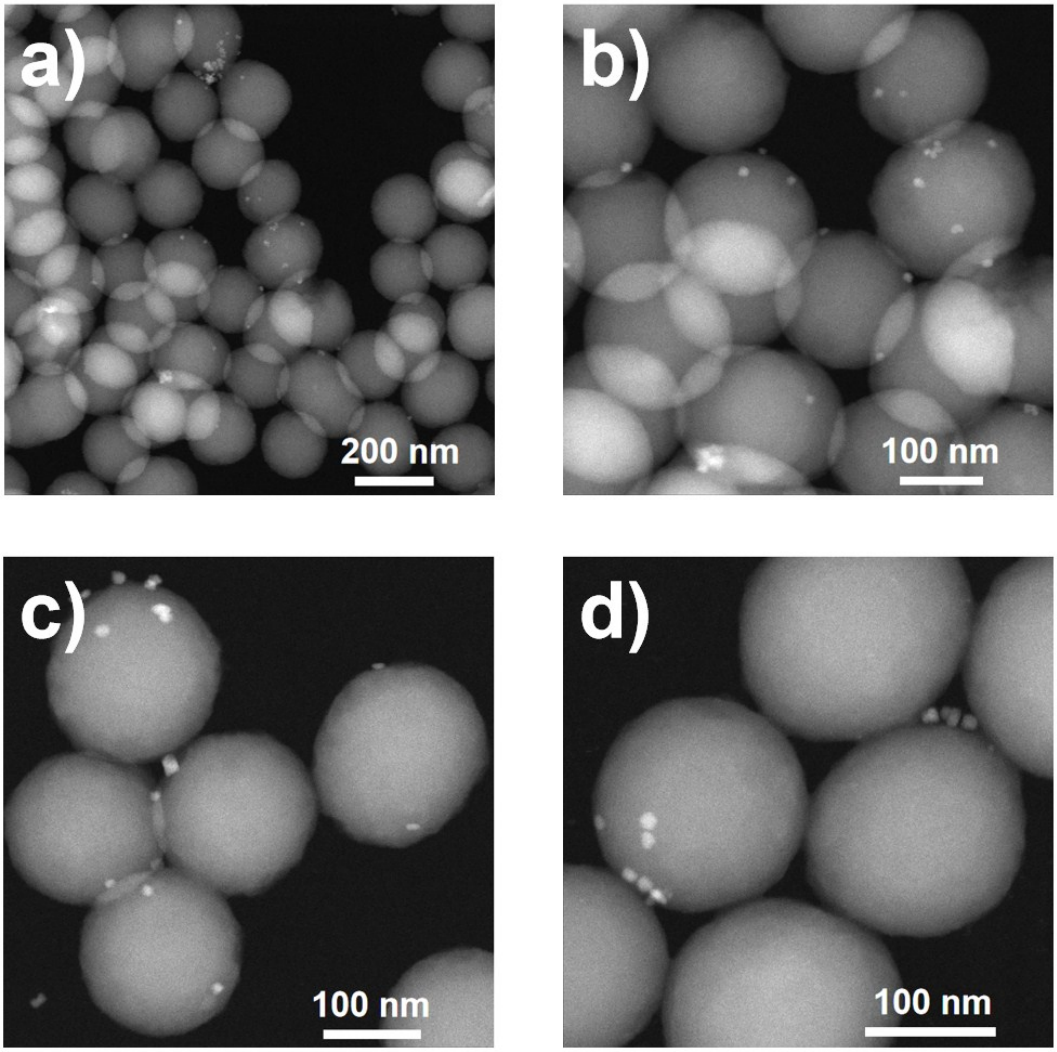

Figure S16. a) - d), High-resolution HAADF-STEM images of Fe-NPs/CN in randomly selected regions at different magnifications.

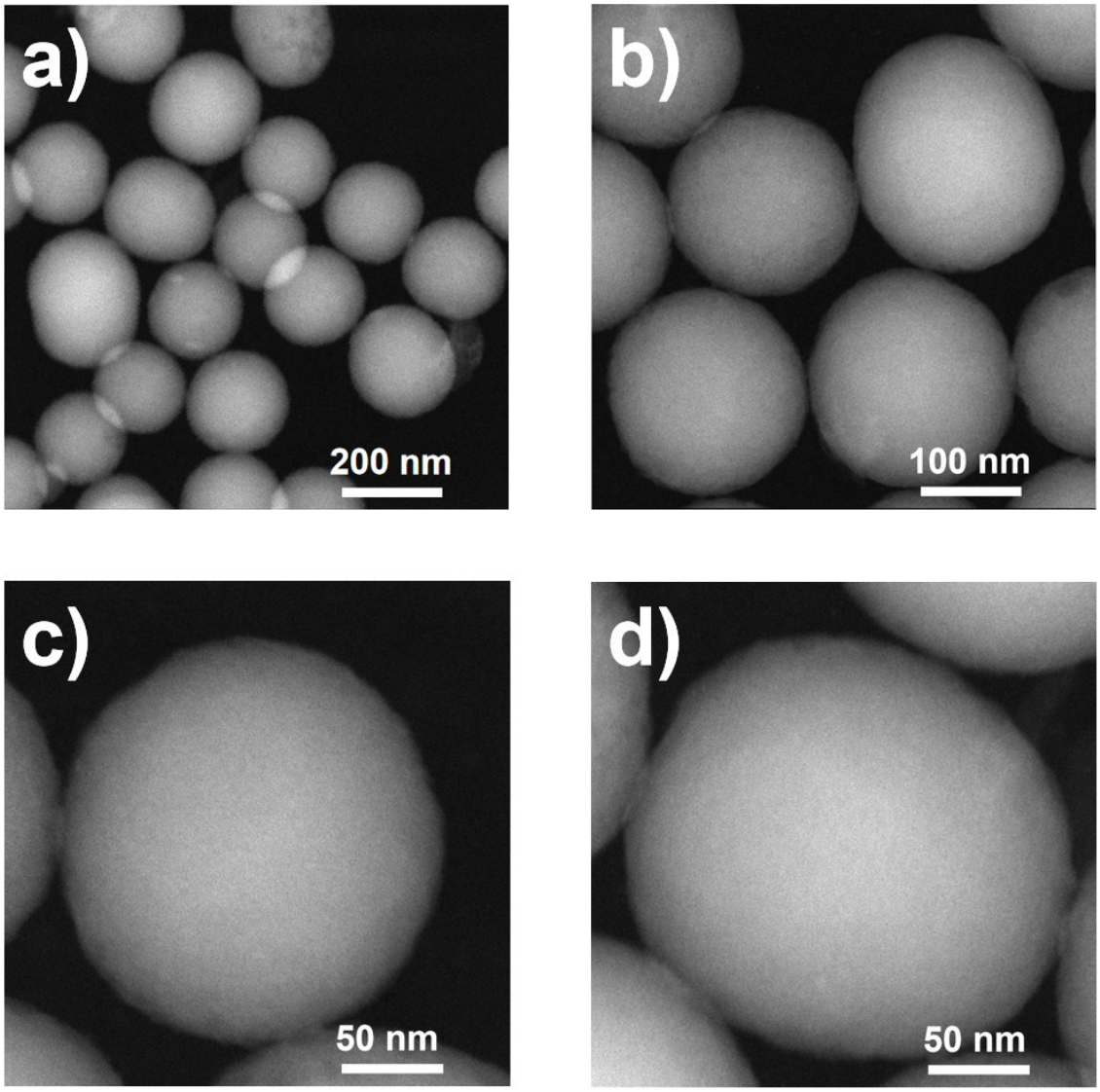

Figure S17. a) - d), High-resolution HAADF-STEM images of Fe-ISAS/CN after cycling in the selective oxidation of ethylbenzene in randomly selected regions at different magnifications.

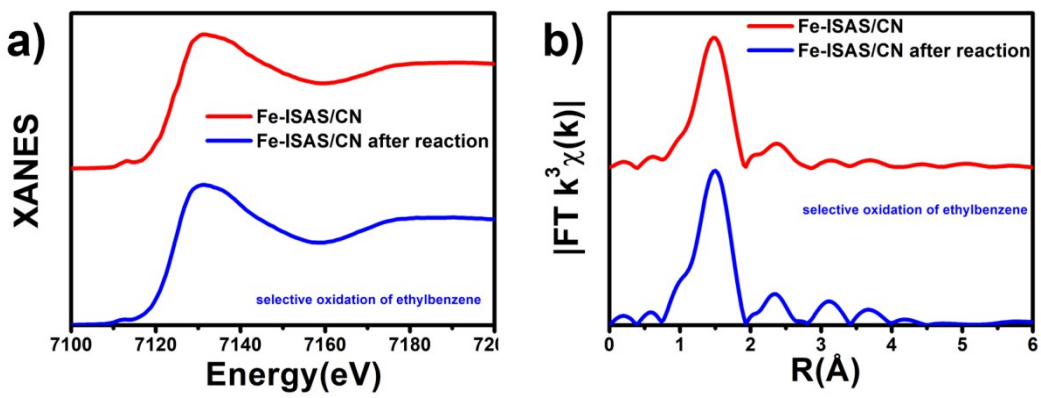

Figure S18. a) - b), The XANES spectra of Fe-ISAS/CN before and after the cycling of selective oxidation of ethylbenzene and corresponding FT-EXAFS spectrum in R space.

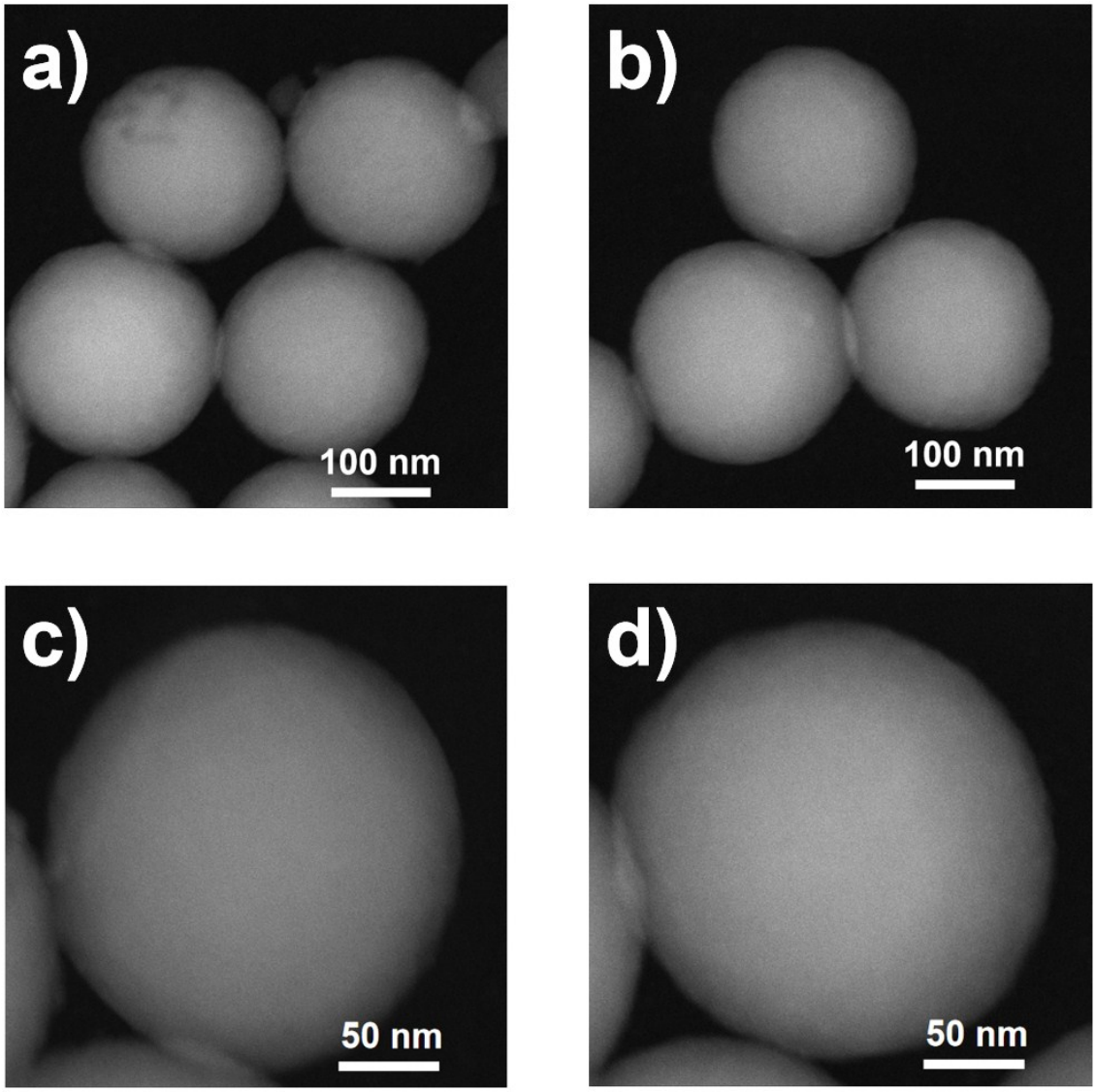

Figure S19. a) - d), High-resolution HAADF-STEM images of Fe-ISAS/CN after cycling in the dehydrogenation of 1,2,3,4-tetrahydroquinoline in randomly selected regions at different magnifications.

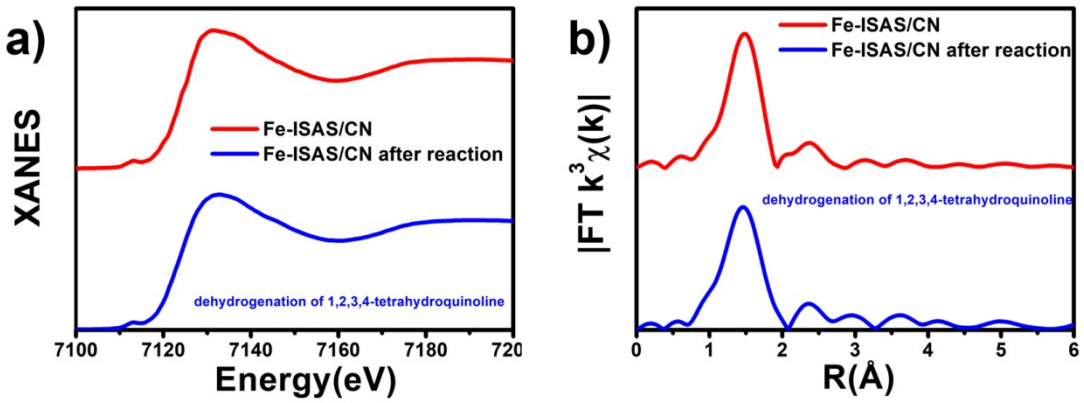

Figure S20. a) - b), The XANES spectra of Fe-ISAS/CN before and after the cycling of dehydrogenation of 1,2,3,4-tetrahydroquinoline and corresponding FT-EXAFS spectrum in R space.

Table S1 Inductively coupled plasma optical emission spectrometry (ICP-OES) measurement.

Sample	The metal content (wt%)
Fe-ISAS/CN	0.046
Co-ISAS/CN	0.11
Ni-ISAS/CN	0.13
Fe-NPs/CN	0.28

Table S2. Structural parameters extracted from the Fe K-edge EXAFS fitting.

(S_0^2=0.85)

Sample	Scattering pair	CN	R(Å)	σ^2(10^{-3} Å^2)	ΔE_0(eV)	R factor
Fe-ISAS/CN	Fe-N/C	4.1	2.01	6.4	1.5	0.006

S_0^2 represented the amplitude reduction factor; CN represented the coordination number; R was interatomic distance (the bond length between central atoms and surrounding coordination atoms); σ^2 was Debye-Waller factor (a measure of thermal and static disorder in absorber-scatterer distances); ΔE_0 represented edge-energy shift (the difference between the zero kinetic energy value of the sample and that of the theoretical model). R factor was used to value the goodness of the fitting. Error bounds which characterized the structural parameters obtained by EXAFS spectroscopy were estimated as N ± 20%; R ± 1%; σ^2 ± 20%; ΔE_0 ± 20%.

Table S3. The comparison of ORR catalytic performance between Fe-ISAS/CN and other reported Fe-based electrocatalysts.

electrocatalysts	**$E_{1/2}$ (V vs. RHE)**	**reference**
Fe-ISAS/CN	0.861	This work
Fe-N-C HNSs	0.87	*Adv. Mater.* **2018***,* 1806312.
p-Fe-N-CNFs	0.82	*Energy Environ. Sci.* **2018**, *11*, 2208.
Fe2-Z8-C	0.87	*Angew. Chem. Int. Ed.* **2018***, 57*, 1204.
Fe-N-DSC	0.83	*ACS Nano* **2018**, *12*, 208.
FeSAs/PTF-600	0.87	*ACS Energy Lett.* **2018**, *3*, 883.
S,N-Fe/N/C-CNT	0.85	*Angew. Chem. Int. Ed.* **2017**, *56*, 610.
Fe-ISAs/CN	0.900	*Angew. Chem. Int. Ed.* **2017**, *129*, 7041.
Fe-NMCSs	0.86	*Adv. Mater.* **2016**, *28*, 7948.
Fe_3C@Fe-N-doped CNFs	0.82	*Angew. Chem. Int. Ed.* **2015**, *127*, 8297.
Fe-N/C catalyst	0.809	*J. Am. Chem. Soc.* **2014**, *136*, 1102.
Fe@C-FeNC-2	0.899	*J. Am. Chem. Soc.* **2016**, *138*, 3570.
Fe-N_4 SAs/NPC	0.885	*Angew. Chem. Int. Ed.,* **2018**, *57*, 8614.

Table S4. The comparison of catalytic performance for the selective oxidation of ethylbenzene toward acetophenone with TBHP in the aqueous phase between Fe-ISAS/CN and other reported catalysts.

Catalyst	**Temp.(°C)**	**Con.(%)**	**Sel.(%)**	**TOF(h^{-1})**	**reference**
Fe-ISAS/CN	60	99	99	125	This work
Mn-Ti/SBA-15	80	92	87	---	*Catal. Sci. Technol.* **2013**, *3*, 2340.
Co/oxide	120	69.5	80.4	5.1	*Catal. Sci. Technol.* **2015**, *5*, 540.
Cu-BTC-SiO_2	60	99	99	3.3	*RSC Adv.* **2014**, *4*, 30221.
Au/LDH	140	39	91	5240	*Nat. Commun.* **2015**, *6*, 6957.
Co/AC	80	47.9	83.5	15.7	*Phys. Chem. Chem. Phys.* **2017**, *19*, 4967.
Ag/SBA-15	90	92	99	9.9	*Catal. Commun.* **2012**, *23*, 5.
CoCuAl-LDH/graphene	120	96.8	95.4	6.1	*ChemCatChem* **2016**, *8*, 363.
Co-N-C	80	99	96	27.9	*Appl. Surf. Sci.***2017**, *419*, 98.
Fe−N−C	RT	99	99	24.7	*J. Am. Chem. Soc.,* **2017**, *139*,

					10790.
Co-ISA/CNB	RT	98	99	57.8	*Adv. Funct. Mater.* **2018**, 1802167

Table S5. The comparison of catalytic performance for dehydrogenation of 1,2,3,4-tetrahydroquinoline between Fe-ISAS/CN and other reported catalysts.

Catalyst	**Temp.(°C)**	**Yield(%)**	**reference**
Fe-ISAS/CN	120	100	This work
ISAS-Co/OPNC	120	99.8	*Angew. Chem. Int. Ed.* **2018**, *57*, 11262.
Pd/Rh/PtNPs/SBA15	130	99.9	*J. Am. Chem. Soc.* **2017**, *139*, 18084.
Cp*Ir Complexes	p-xylene reflux	100	*J. Am. Chem. Soc.* **2009**, *131*, 8410.
Ir Complexes	p-xylene reflux	100	*J. Am. Chem. Soc.* **2014**, *136*, 4829.
CuNPs/TiO_2	150	99	*Heterocycles* **2011**, *82*, 1371.
Co-pincer	150	70	*ACS Catal.* **2015**, *5*, 6350.
Pt/C	o-xylene reflux	81	*Catal. Today* **2017**, *281*, 507.
FeOx@NGr−C	100	83	*J. Am. Chem. Soc.* **2015**, *137*, 10652.
CoOx-phen/AB	160	92	*Org. Lett.* **2015**, *17*, 4404.

Supplementary References

[1] D. Rodríguez-San-Miguel, J. J. Corral-Pérez, E. Gil-González, D. Cuellas, J. Arauzo, V. M. Monsalvo, V. Carcelén and F. Zamora, *CrystEngComm*, **2017**, *19*, 4872-4876.

[2] S. Tian, Q. Fu, W. Chen, Q. Feng, Z. Chen, J. Zhang, W.-C. Cheong, R. Yu, L. Gu, J. Dong, J. Luo, C. Chen, Q. Peng, C. Draxl, D. Wang and Y. Li, *Nature Commun.*, **2018**, *9*, 2353-2359.

[3] B. Ravel, and M. Newville, J. *Synchrotron Radiat.* **2005**, *12*, 537-541.

[4] A. L. JAnkudinov, B. Ravel, J. J. Rehr, and S. D. Conradson, *Phys. Rev. B* **1998**, *58*, 7565-7576.